Lab on a Chip

Accepted Manuscript

ROYAL SOCIETY OF CHEMISTRY

www.rsc.org/loc

Lab on a Chip

RSCPublishing

Paper

AC Electric Field Induced Dipole-Based On-Chip 3D Cell Rotation

Cite this: DOI: 10.1039/x0xx00000x

Prateek Benhal [a], J. Geoffrey Chase [a], Paul Gaynor [b], Björn Oback [c], and Wenhui Wang [d]

Corresponding Author E-mail: geoff.chase@canterbury.ac.nz, wwh@tsinghua.edu.cn

Received 00th January 2012,
Accepted 00th January 2012

DOI: 10.1039/x0xx00000x

www.rsc.org/

Precise rotation of suspended cells is one of many fundamental manipulations used in a wide range of biotechnological applications such as cell injection and enucleation in nuclear transfer (NT) cloning. Noticeably scarce from the existing rotation techniques is three-dimensional (3D) rotation of cells on a single chip. Here we present an alternating current (ac) induced electric field-based biochip platform which has an open-top sub-mm square chamber enclosed by four sidewall electrodes and two bottom electrodes to achieve rotation about two axes, thus 3D cell rotation for the first time. By applying an ac potential to the four sidewall electrodes, an in-plane (yaw) rotating electric field is generated and in-plane rotation is achieved. Similarly, by applying ac potential to two opposite sidewall electrodes and the two bottom electrodes, an out-of-plane (pitch) rotating electric field is generated and rolling rotation is achieved. For prompt proof-of-concept, bottom electrodes were constructed with transparent indium tin oxide (ITO) using the standard lift-off process and the sidewall electrodes were constructed with a low-cost micro-milling process, and then assembled to form the chip. Through experiments, we demonstrate rotation of bovine oocytes of ~120 μm in diameter about two axes, with the capability of controlling the rotation direction and rate for each axis through control of the ac potential amplitude, frequency, and phase shift, and cell medium conductivity. The maximum observed rotation rate reached nearly 140 °/s, while a consistent rotation rate reached up to 40 °/s. Rotation rate spectra for zona pellucida-intact and zona pellucida-free oocytes were further compared and found to have no effective difference. This simple, transparent, cheap-to-manufacture, and open-top platform, allows further function modules to be integrated to become a more powerful cell manipulation system.

Introduction

Precise translation and rotation of biological entities, such as spherical cells, are two fundamental manipulation requirements in applied biotechnological research [1-9]. Unlike translational manipulation, for which a number of methods and devices are available to actuate three-axis displacements, rotation remains extremely challenging when it is required for more than a single axis of cell orientation in 3D spaces. Two typical case applications are cell injection and enucleation, which can be roughly thought of as two reverse manipulations in order [10-14]. As common practice in biology laboratories, cell injection uses a glass micropipette to *deposit* foreign materials into a desired destination of a cell [15]. In contrast, enucleation uses a glass micropipette to *extract* DNA materials out of the recipient cell in NT cloning technology [10, 12, 16-19]. For both manipulations to achieve high performance, it is imperative to align the selected injection point or DNA material with respect to the glass micropipette. As the injection point or DNA material of a cell is initially located at an arbitrary orientation, the cell has to be rotated about more than one axis in order to achieve appropriate alignment.

Manual rotation using the micropipette tip to manipulate the cell is commonly adopted in laboratory [13, 20]. Due to the human labour nature, this method has inherent disadvantages such as low efficiency, poor precision and inconsistent performance. These disadvantages drive researchers to leverage a range of physical phenomena and propose corresponding methods for cell rotation, such as electro-kinetics [21, 22], optical tweezers [23] and

micro-fluidics [24-26]. In general, the majority of microchips work on existing methods include electric torque induced by dielectrophoresis (DEP) [2, 27-31], and optoelectronic torque induced by optical means coupled with DEP such as optical tweezers and ODEP [32]; while a few include magnetic torque and mechanical torque. All these methods have been demonstrated to be capable of rotating cells, whose size ranges around 10 μm in diameter. However, scarcely seen is the controlled rotation of cells in 3D space or controlled rotation about more than one axis in one single device, which is the most important issue to be addressed in this paper.

DEP has been widely attempted for trapping, translating and rotating cells [21, 28, 33-37]. Subjected to a non-uniform electric field, any polarizable entity, which includes cells, experiences locally-concentrated induced electric dipoles, which in turn undergo electric forces or torques in the electric field. Collectively, a net DEP force or torque is generated on the cell, leading to translation or rotation respectively. Based on this phenomenon, a classic method was reported to rotate cells in a chamber enclosed by four vertical electrodes, both theoretically and experimentally [36, 38-42]. This early implementation applying external ac potential or direct current (dc) potential alternatively to the vertical electrodes achieved in-plane (yaw) rotation about one single axis, leaving the rotation about multiple axes still a problem.

Recent research has brought a new element into DEP by introducing an optical means to induce DEP and this can be called optical DEP (ODEP) [21, 25, 32]. Compared to conventional DEP, ODEP differs in applying the potential to electrodes by light induced electric field instead of an external potential source. The disadvantages of this technique, however, include three aspects: i) The rotation is still only about a single axis. ii) To induce the rotation, a top electrode is necessary, leading to a closed rotation chamber which hampers external access to the cell inside. iii) The ODEP technique has not been tried on larger size cells of around 100 μm.

Another similar method is based on optical tweezers, which use the optoelectronic torque generated in the focal point of a light beam to trap and rotate particles [23, 43, 44]. Due to the limited energy of the light, like ODEP the torque is normally insufficient to rotate cells above 10 μm level. In contrast, optical tweezers are very suitable for rotating particles of 1-10 μm level. Additionally, rotation of particles about more than one axis using optical tweezers has not yet been reported.

Magnetic fields have also been used to rotate cells. Initially, housed in a chamber enclosed by vertically configured electromagnets [45, 46], magnetic beads are solely rotated in-plane. Recently, researchers embedded magnetic nanoparticles into cells, which underwent a magnetic torque in a rotating magnetic field and thus rotated [47] in-plane about the Z-axis (with axis orientation as identified in Fig. 1). This method involves inserting magnetic nanoparticles into cells. As an invasive sample preparation step, it raises the risk of cell damage and may interfere with the cell viability and development, and thus has limited practical application.

Based on the above analysis, a method that solely uses ac electric fields for dual axis rotation is proposed in this paper. Relatively higher torque induced by a rotating ac electric field is taken advantage of rather than ODEP or optical tweezers, allowing rotation of cells larger than normal, such as bovine oocytes used in cloning studies, which are typically more than 100 μm in diameter [13]. Accordingly, to realize dual-axis rotation, our biochip differs from existing micro-devices in that it integrates six electrodes, which are arranged on the bottom substrate and sidewalls, whereby dual-axis rotation is controlled by varying applied ac potential amplitude, frequency, and phase shift. In particular, the in-plane (yaw) rotating electric field is generated by solely activating sidewall electrodes and vertical out-of-plane (pitch) rotating electric field by activating bottom electrodes and one opposite pair of vertical electrodes. In MicroTAS 2013 [48], we have reported our progress in fabrication of a proof-of-concept biochip and the preliminary experimental data for bovine cell rotation. Here, in this paper, we fully describe the biochip design, working principle, and fabrication; and show more experimental results to characterize the dual-axis rotation of bovine oocytes. Our chip is transparent, cheap-to-make, and open-top, rendering its potential capability of rotating cells in 3D space for applications such as cell injection/enucleation, cancer cell identification, cell dielectric property measurement, and 3D cell imaging. As the applied ac electric field induced dipoles are universal in any polarizable material, the biochip could be extended to rotate entities such as beads, particles, DNA, proteins, and larger organisms.

Chip design and fabrication

Chip layout

Fig. 1 illustrates the biochip, which essentially consists of six electrically-isolated electrodes sitting on a glass slide. Four sidewall vertical electrodes are used to induce yaw rotation; while the two bottom electrodes, together with the sidewall electrodes, are used to induce pitch rolling rotation. Here, the novelty lies in sharing the sidewall electrodes for pitch rolling rotation, leaving an open top to the biochip chamber, where the cell is contained. Sharing the sidewall electrodes simplifies the biochip structure, while the open top provides external access to the cell – where both features have a favorable benefit for subsequent cell manipulation, for example, through a micropipette or further integrating with microfluidic channels.

The sidewall electrodes are separated by a layer of insulator from the bottom electrodes to avoid an electrical short. Also, to allow easy observation into the biochip chamber, the bottom electrodes are chosen to be transparent indium tin oxide (ITO). As bovine oocytes are our first interest in research, the height and length of the sidewall electrodes are chosen to be 500 μm and 750 μm respectively to form a chamber with a suitable manipulation space for a cell of ~120 μm in diameter. Through parametric finite element analysis (FEA) of rotational electric field studies (results not shown in this paper), it was determined that a square

chamber area of 750 μm × 750 μm provides sufficient rotational field strength in the order of 10^4 V/m magnitude to rotate ~120 μm sized cells when using standard signal generation apparatus, and is relatively easy to manufacture using facilities in our lab. Since chamber size may not be highly important with regards to initial observations of 3D rotation, we did not test smaller chambers. This first-of-its-kind 3D cell rotation biochip platform looks simple, however, it is this rather simple structure that offers future opportunities to integrate more structures or tools on top of it and thus expand its usability.

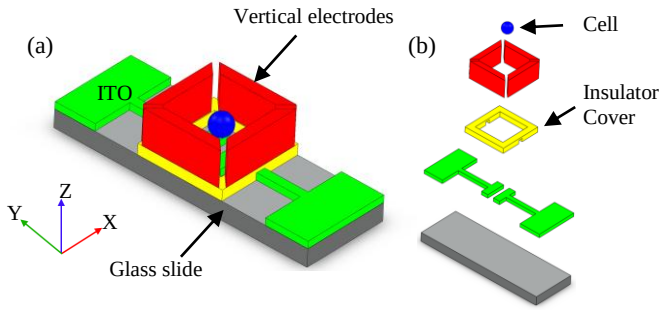

Fig. 1: DEP biochip platform design. (a) Overview. (b) Exploded view: four isolated vertical electrodes (red) of 750×750×500 μm in width, length and height, forming a chamber with a cell (blue) inside and two bottom ITO electrodes (green - 250 μm×500 μm×100 nm each in width, length and thickness) separated by a 30 μm gap. The vertical electrodes are isolated from the bottom electrodes via a plastic insulator layer (yellow –film made of mylar) of 25 mm×25 mm×12 μm in width, length and thickness. **Dimensions not to scale.**

Biochip working principle for 3D cell rotation

In this paper, cell rotation is based on the ac potential induced rotating electric field. For the four sidewall electrodes, it is well known that by applying ac potential with a 90 ° phase shift, an in-plane rotating electric field is generated, in particular in the central region of the chamber enclosed by the four electrodes. Simulations were conducted to verify the phenomenon with FEA software (COMSOL V4.3). Simulations were also conducted to investigate how to generate a rotating electric field for out-of-plane rolling rotation using two sidewall electrodes and two bottom electrodes.

Fig. 2 shows the ac potential schemes for rotations about the Z-axis (in-plane, top view) and X-axis (out-of-plane, side view) respectively. For in-plane rotation, ac potentials with equal amplitude but with 90 ° phase shift are applied to only the four sidewall electrodes, leaving the bottom electrodes electrically floating. The potential scheme is shown in Fig. 2a where the generated in-plane rotating electric field (anti-clockwise) in one period is apparent. If the order for the ac potentials applied to the four electrodes is changed, the in-plane rotating electric field changes its direction to being clockwise. This is the way we control the cell rotation direction.

For pitch rolling rotation, ac potentials with equal amplitude are applied only to the bottom electrodes, leaving the two neighbouring sidewall electrodes grounded and the other two floating. The potential scheme is shown in Fig. 2b and the generated rotating electric field (clockwise) about the pitch X-axis in one ac period is apparent. Note the phase shift between the two bottom electrodes is now 50 °, not 90 °. This is because with 50 ° phase shift, the rotating electric field occupies a larger region with less-variation in strength, which would result in a more stable rotation. Similarly to in-plane rotation, if the order for the ac potentials applied to the four electrodes is changed, the rotating electric field about the X-axis changes its direction to anti-clockwise.

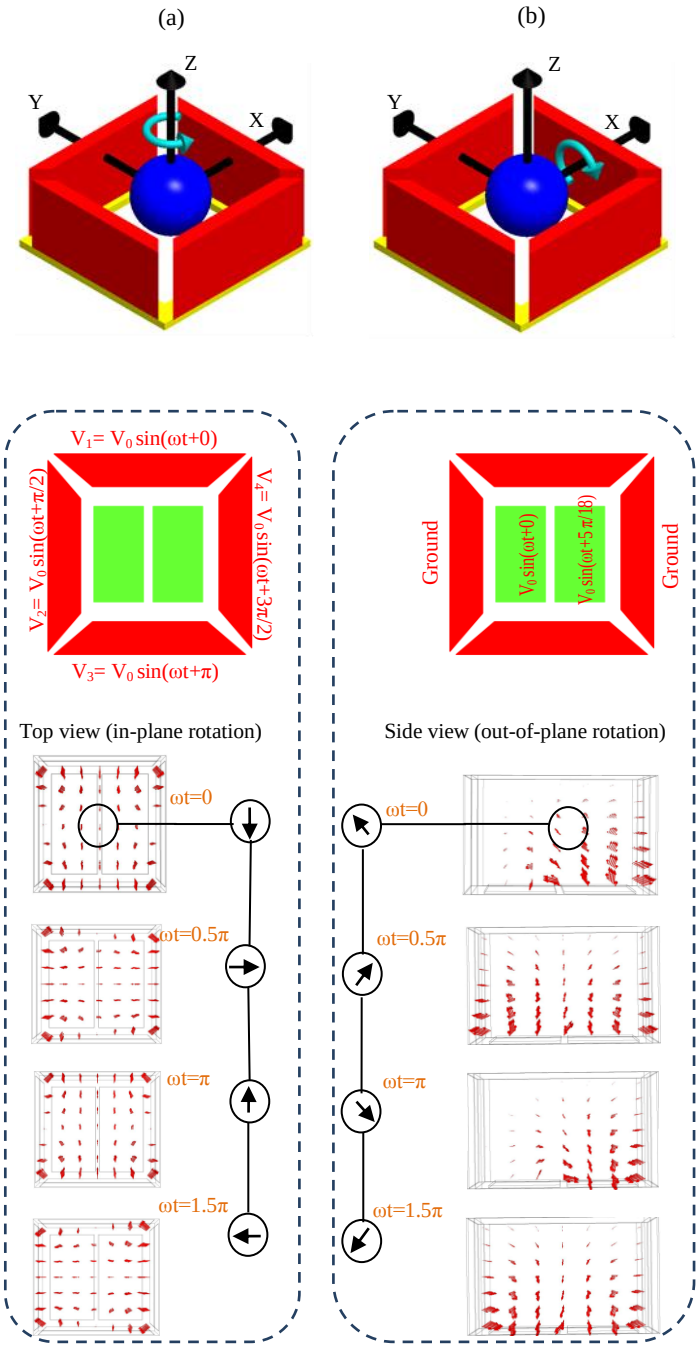

Fig. 2: Electric field analysis. (a) In-plane (yaw) rotation: top view. (b) Out-of-plane (pitch) rotation: side view. The first row shows 3D illustration of the rotation about two axes. Complete rotation of electric field for a single period of ωt=0 to 1.5π, using COMSOL v4.3 FEA software. ω-angular frequency of the applied ac electric field and t-time in seconds. Arrow vectors length and thickness correspond to field strength.

Under a rotating electric field, a spherical dielectric particle is subjected to a torque, which is defined as [49, 50]:

$$T = 4\pi\varepsilon_m R^3 \mathrm{Im}[f_{cm}]E^2 \quad (1)$$

where ε_m is the complex medium permittivity (a frequency-dependent complex value), R is the radius of the particle, $Im[]$ stands for the imaginary part of a complex variable, E is the electric field magnitude, and f_{cm} is the Clausius-Mossotti (CM) factor that characterizes the frequency-dependent dipole moment:

$$f_{cm} = (\varepsilon_p - \varepsilon_m)/(\varepsilon_p + 2\varepsilon_m) \quad (2)$$

Where, ε_p is the particle complex permittivity.

If a constant angular velocity (Ω) of a particle is assumed, then the hydrodynamic torque T_f arising from the Stokes drag force is given by [3]:

$$T_f = 8\pi\eta\Omega R^3 \quad (3)$$

where η is the viscosity of the medium.

In equilibrium, $|T|=|T_f|$. Using Eqs. (1) and (3) we then have

$$\Omega = \varepsilon_m/(2\eta)\mathrm{Im}[f_{cm}]E^2 \quad (4)$$

Equation (4), along with Eq. (2), indicates that the particle steady angular speed is dependent on the medium and particle's electrical properties, the electric field magnitude and frequency, the position of particle in the chamber, and the structure of the biochip electrodes. These factors provide the ability to control speed and direction of particle rotation. The rotation spectrum of a homogenous isotropic spherical particle has a single peak at the Maxwell-Wagner frequency.

Biochip fabrication

This paper aims to demonstrate that the biochip platform works for 3D cell rotation, therefore although it is possible to fabricate the entire biochip through photolithography technology which facilitates very good miniaturization and electric interfaces, photolithography was not adopted for fabricating the sidewall electrodes in order to avoid unnecessary difficulty. Instead, as shown in Fig. 3, the sidewall electrodes were fabricated by micro-milling and the bottom electrodes by photolithography, respectively. Then the parts are assembled to form the biochip platform. In this way, we saved time and cost while still obtaining a workable chip. The fabrication process is described in brief (Fig. 3).

To fabricate the bottom electrodes on borosilicate glass, the simple and standard life-off process [51] was used (details are omitted here). The sidewall electrodes are micro-milled using a Mini-Mill/GX CNC machine (Mini Mill/GX^{TM}). In particular, a brass strip of 500 µm in thickness is cut to 25 mm square and adhered onto PMMA which serves as a support base for the subsequent micro-milling. Along the diagonals of the square, the brass layer is micro-milled into four electrically-isolated parts, which serve as the four sidewall electrodes. In micro-milling, a cutting spindle speed of 30,000 rpm and a feed rate of 0.6-1.2 µm/s was found effective to mill the brass strip. Around the intersection point of the diagonals, a circular through-hole of 750 µm in length is formed by a drilling tool in the same micro-milling machine at 7000 rpm spindle speed through the PMMA, serving as the access area to the rotation chamber for loading/unloading bovine oocytes.

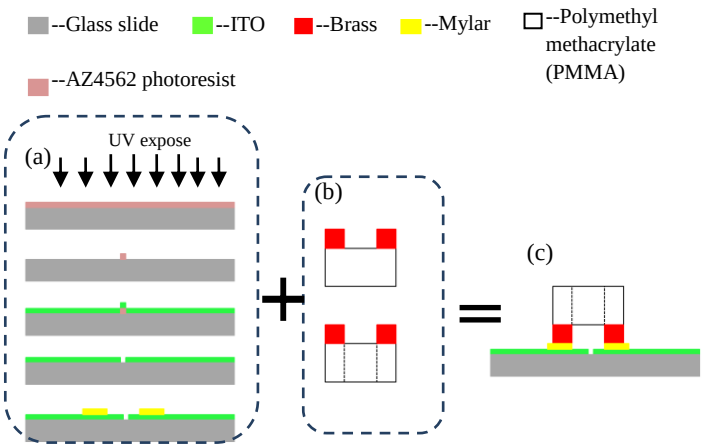

Fig. 3: Fabrication process of biochip. (a) ITO-patterned glass slide through standard lift-off process [51] and an insulator layer made of 25 mm×25 mm×12 µm in width, length and thick, mylar film. (b) Micro-milled brass fixed on top of polymethyl methacrylate (PMMA) with PMMA adhesive as vertical electrodes and through-hole in the PMMA. (c) Assembly. **Figure not to scale.**

The micro-milled part is then inverted and placed on top of the electrode-patterned glass slide. In between is sandwiched a transparent plastic cover slip (fabricated from mylar film) of 12 µm thickness. The cover slip is a 25×25 mm square ring. It serves as both an electrical and thermal barrier between the sidewall and bottom electrodes. Finally, the biochip is mounted on a custom made support and suitable electrical connections are wired to an external potential supply for the six electrodes. A picture of the biochip platform is shown in Fig. 4.

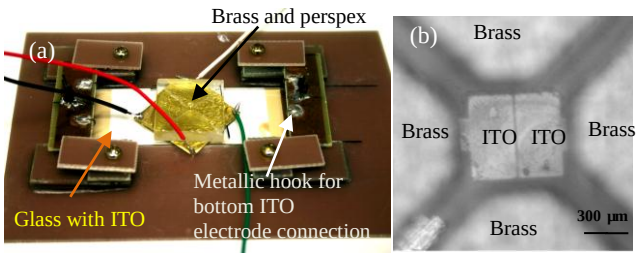

Fig. 4: Fabricated biochip. (a) Fabricated biochip with electrical connections. (b) Close-up top view shows sidewall brass and bottom ITO electrodes. The chamber workspace is a 750-µm square area [48].

Experiments

Materials and method

Oocytes were collected from abattoir ovaries and manipulated as described [12]. Briefly, metaphase-II oocytes are treated with hyaluronidase to remove cumulus cells surrounding the oocyte. The outer protein shell, called the zona pellucida (ZP), was either left intact or enzymatically removed with pronase to obtain ZP-free oocytes. Sterile HSOF solution is used to wash the oocytes. ZP-free and ZP-intact oocytes are then kept at room temperature in a 13 mm Vacutainer containing embryo holding media [13].

The buffer medium in all experiments was hypoosmolar, consisting of 0.05% bovine serum albumin, 200 mM mannitol, 50 μM $CaCl_2$, 100 μM $MgCl_2$, and 500 μM Hepes [52]. Electric conductivity of the buffer was measured using a pH/conductivity meter AP85 (Fisher Scientific). In experiments, the fabricated biochip was submerged in a Petri dish containing buffer solution. Oocytes were then manually transferred via a mouth pipette into the biochip chamber. During each experiment, a bovine oocyte was slowly and carefully injected manually into the rotation chamber from a micro-pipette (mouth-pipetting) through the hole in the PMMA top layer. The following protocols are precisely adhered to when positioning an oocyte in the rotation chamber to maximize reproducibility:

- A single bovine oocyte is selected by mouth pipetting.
- Slowly and carefully the single oocyte is placed at the centre of the hole. During this phase, a camera interfaced with the inverted microscope is used to feedback the oocyte position.
- Within 5-10 seconds the oocyte settles down at the centre of the rotation chamber due to gravity and the suspension/buffer medium density and viscosity.
- The proper suspension of the bovine oocyte was checked by focusing on the bottom electrodes and the cell rim respectively under 40x microscope objective.

Experimental setup

An inverted epi-fluorescent microscope (Nikon Eclipse 80i) sits on a pneumatically controlled anti-vibration table (TMC, USA). The Petri dish housing the biochip is placed on the microscope stage, with electric wires connecting to a four-channel TGA1240 series 40MHz arbitrary waveform generator, which supplies phase-shifted ac potentials to the electrodes in accordance with the biochip working principle. A CCD camera (Nikon Eclipse DS-Fi2) is mounted on the microscope to record and image the cell rotation in bright-field mode at 10×. A desktop computer is interfaced with the camera to capture video and images.

Experimental data collection and analysis

Video clips during experiments are captured with f=30 Hz sampling frequency for each individual oocyte. These video frames are processed offline to estimate the cell rotation rate manually using the free software ImageJ V1.46r manual tracking plugin, NIH, USA. The estimation methods for two-axis rotation have to be different, because the cell has completely different motion patterns and observable features.

In particular, when the cell has an in-plane rotation, it is like a flat disk rotating about its center. Using this observation, a line was successfully drawn in each video frame connecting two consistent reference points on the cell, one being the cell center and the other a feature point on the circumference of the cell. The angle between this line and the horizontal line is denoted by θ. The change in θ between each two successive frames is denoted by $\partial\theta$, then the rotation rate can be given by $\Omega=\partial\theta/\Delta t$, where Δt is the sampling period ($\Delta t=1/f$=0.033 s). In practice, to accommodate the case when $\partial\theta$ is immeasurable, the angle change in several successive frames was used and this is divided by that time interval for the yaw rotation rate Ω.

In the cases when feature points are hard to determine on the cell (Fig. 5b), the video files are imported into ImageJ and each frame is further processed to determine several pixel points on the circumference of the oocyte. The obtained key points are manually tracked by using the Manual Tracking plug-in tool. A detailed procedure to calculate the rotation measurement is provided in the supplementary information 1 (SI 1).

When the cell has a rolling rotation, due to its extremely complicated texture, it is not possible to choose a feature point with unique grey-level properties, making the previous method of tracking feature points invalid. To estimate the rotation rate, we assume the cell rolls without any sliding. With this assumption, the distance (denoted by d) the cell travels between two successive frames was measured. Then the rotation rate can be given by $\Psi=d/(r\cdot\Delta t)$, where r is the cell radius. In practice, similarly to in-plane rotation, to accommodate the case when d is immeasurable, the distance in several successive frames were used and divided by that time interval for the pitch rotation rate Ψ.

Results and discussion

Healthy bovine oocytes were used in experiment to demonstrate cell rotation. Each time, a single oocyte was loaded in the biochip chamber with buffer solution media. Care was taken to gently manipulate the oocyte with the mouth pipette so that it was located in the central region of the chamber as the start position. Sufficient time was given for the oocyte to settle in the media to make sure it reached a suspension steady-state which was above, and not in contact with the chamber bottom surface. For any oocyte that sank to the bottom, it was removed from the chamber because the friction between the oocyte and the bottom surface would have an effect on the rotation properties.

Once ready, an individual bovine oocyte was rotated in-plane when the four sidewall electrodes had ac potentials applied in accordance with the configuration in Fig. 2a. When two sidewall electrodes and the bottom electrodes had ac potentials applied in accordance with the configuration in Fig. 2b, the oocyte rotated out-of-plane in a rolling pattern. Rotation initiation and termination were triggered by switching the ac potentials on and off respectively. The rotation data were collected for varying frequency in the range of 10 kHz-10 MHz and two amplitudes of

10 V and 20 V. In total, 24 oocytes were tested and their rotation spectra about both axes against factors like frequency, ac potential amplitude, and medium conductivity were obtained. Note, we did not characterize the effect of the cell size on rotation in this paper.

Bubble formation of some sort is common during most electric cell manipulation experiments. To help avoid this issue, the entire biochip was completely air sealed by submersion in the buffer medium. A small amount of bubble generation was however seen in experiments where signals with frequencies below 10 kHz for both 10-20 Vp-p were applied. For experiments using signals between 10 kHz to 5 MHz for 10-20 Vp-p, bubble formation was not witnessed. Overall, bubble formation was not an issue during experiments.

In-plane (yaw) rotation of individual oocytes

Firstly, individual bovine oocytes were rotated in the biochip chamber through applying ac potentials to the four sidewall electrodes. When the amplitude was below 10 V, no rotation was observed in the adjustable frequency range of 10 kHz-10 MHz. However, clockwise rotation of the oocyte was observed when the amplitude reached 10 V, as shown in the first row of Fig. 5a and Fig. 5b. During the course of rotation, the cell was relatively steady in terms of its relative location in the biochip chamber and its rotation rate for a particular frequency setting. When increasing the frequency in the adjustable range from 10 kHz to 10 MHz, change in the rotation rate was observed, but no change in the rotation direction. This observation holds true for all oocytes in experiment.

Next, oocytes were rotated in the opposite direction (anti-clockwise) by simply reversing the phase of the ac potentials on the four sidewall electrodes. The above observations for clockwise rotation of the oocytes remained the same with the only exception being a resultant anti-clockwise rotation, as shown in the second row of Fig. 5a and Fig. 5b. No measurable difference in the rotation rate between the clockwise and anti-clockwise directions under the same settings of frequency and amplitude was observed. We were also able to instantaneously start and stop rotation (See SI 2 for more information), demonstrating the controllability and flexibility of cell rotation.

For the oocytes in experiment, rotation was observed at frequencies between 100 kHz and 10 MHz. In particular, oocytes rotated most consistently at the centre of the biochip chamber at 500 kHz. The oocyte retained its morphology during this flat-disk (yaw) spinning. The minimum rotation rate of 17 °/s was observed in experiment, and thus the angle change between two successive frames can be calculated to be 17 °/30 = 0.57 ° on average. The angle between two successive frames corresponds to the minimum angle resolution which could be achieved for computer control, if we use 30 Hz video as on-line visual feedback.

To characterize the effects of factors such as frequency, amplitude, and medium conductivity on the bovine oocytes, three to four oocytes were tested under each combination of these factors and the results are shown in Fig. 6.

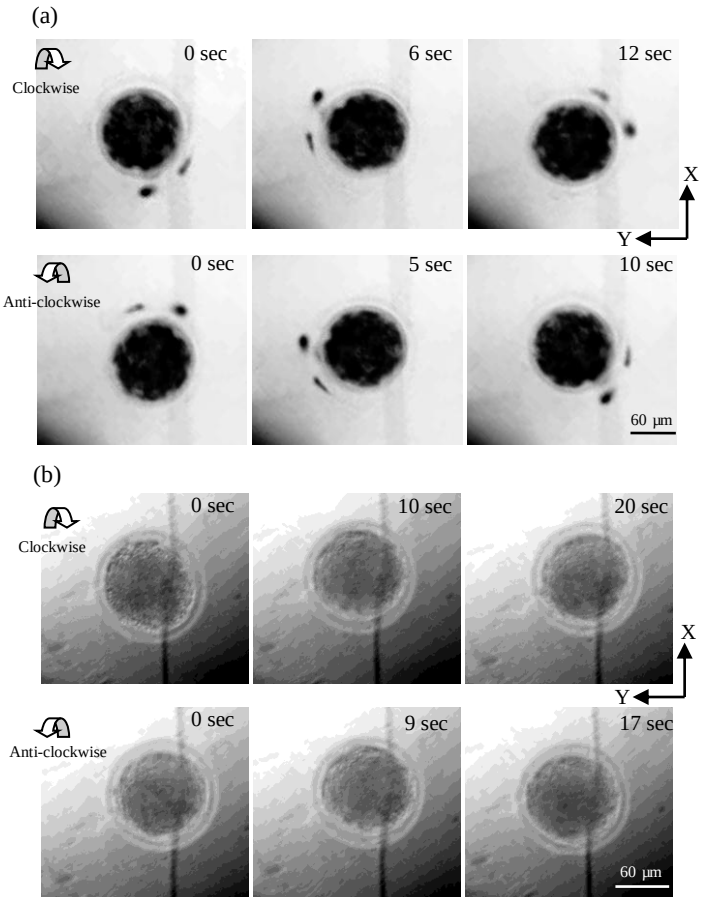

Fig. 5: Snapshot of individual bovine oocyte yaw rotation in experiment. Arrows show the rotation direction. Settings for (a) ZP-free oocyte rotation and (b) ZP-intact oocyte rotation, at 10 V, 500 kHz frequency and 90 ° phase shift between two pairs of orthogonally arranged vertical electrodes.

Four significant observations are: i) The rotation rate versus frequency curve has a characteristic similar to a band-pass filter. At the low and high frequency regions, oocytes do not rotate at all; in the central frequency range the oocytes rotate first faster as the frequency increases and then slow down as the frequency increases further – with a Gaussian curve characteristic. There exists only one peak rotation rate (138 °/s for an amplitude of 20 V, and ~90 °/s for 10 V) in the measured frequency range. ii) Higher potential amplitude (and hence higher electric field magnitude) results in a faster rotation, which is evident if comparing the data points for 10 V and 20 V. The latter voltage led to nearly 1.5 times increase in rotation rate. iii) Applied with higher amplitude potentials, the rotation rate increases to its peak at a lower frequency. This is evident if the data points for 10 V and 20 V are again analysed. The 20 V experiments yielded a peak rotation rate at about 1 MHz, whereas the 10 V experiments yielded a peak rotation rate at about 2 MHz. iv) Although, at the two low media conductivities used, no difference in rotation rate is observable (Fig. 6), additional experimental work was carried out to determine the effect of different medium conductivity on oocyte rotation. These four significant findings are valuable for guiding the design of control scheme of cell rotations in various applications.

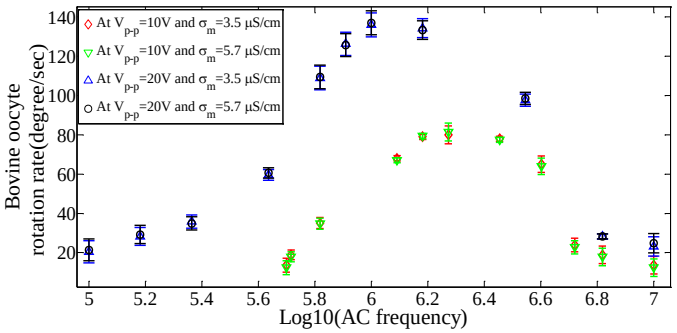

Fig. 6: ZP-free bovine oocyte in-plane rotation rate in relation to the conductivity (σ_m) of buffer medium and the applied ac potential (frequency and amplitude Vp-p) in experiment. Based on 4 oocytes × 3 replicates (N=4, n=3) with N being the number of samples and n being the number of technical replicates.

The effect of medium conductivity on the rotation rate was further analysed in detail. Because the medium used has a wide possible conductivity range, the value selected being determined by various biological applications. Due to the medium availability, the same type of buffer medium was used, but with different conductivity. At the same time, the potential amplitude was restricted to 10 V to minimize cell lysis. Under these conditions, Fig. 7 shows the rotation rate spectrum of four single oocytes at different medium conductivity. Note that different oocytes were used to generate the data in Fig. 6 and Fig. 7. Hence, owing to unavoidable biological and experimental variation, the results are non-identical between Fig. 6 and Fig. 7. It can be seen that the rotation rate increases very slightly as medium conductivity increases, which is consistent with the theoretical analysis and findings in literature [53, 54]. In contrast to the effect of the potential amplitude, the change in medium conductivity does not change the rotation rate in a comparable manner. It should be noted that when the medium conductivity is higher, the buffer medium becomes less viscous, lowering the oocyte suspension success rate. When the medium conductivity is lower, the buffer medium becomes more viscous, making it more difficult to transfer oocytes. As such, this change in medium viscosity with change in conductivity is the most likely reason for the observed minor change in rotation rate related to medium conductivity.

It is worth mentioning at this point that cell lysis (loss of membrane integrity) was occasionally observed at higher frequencies. When the potential amplitude was set at 20 V, the minimum frequency that would cause cell lysis was 1 MHz. When the potential amplitude was set at 10 V, the minimum frequency that would cause cell lysis was about 2 MHz. Furthermore, it was observed that oocytes were more likely to lyse when the frequency exceeded 5 MHz for both 10 V and 20 V.

Rolling out-of-plane (pitch) rotation of bovine oocytes

Similarly to the in-plane rotation experiments, we managed to pitch-rotate oocytes by applying ac potentials to the bottom electrodes, grounding their neighbouring two sidewall electrodes, and leaving the remaining two sidewall electrodes floating. In comparison to in-plane rotation, the bovine oocyte started to roll in the y-direction about the pitch (x) axis with a potential of 10 V amplitude and 10 kHz frequency. At 10 V, the rolling rotation was very gentle. On or above 15 V, the rotation was more significant with a faster rate.

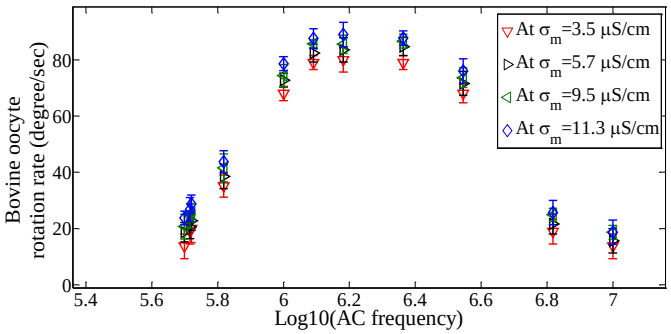

Fig. 7: ZP-free bovine oocyte in-plane rotation rate in relation to the conductivity (σ_m) of buffer medium and the applied frequency in experiment. Here the ac potential amplitude is fixed at 10 V. Based on N=4, n=3. For each frequency, 12 data points from media in different conductivity were analysed by the 2-tailed t-test with equal variance.

Note the rolling pitch rotation had a different pattern than the in-plane rotation in that the cell rolled over like a running wheel. Due to the lack of unique feature points on the rolling oocyte, the rotation pattern shown as top view in Fig. 8 looks as if the oocyte translated to the left (Fig. 8a) and the right (Fig.8b) along the Y-axis. However, the time-varying textures of the oocyte indicate its rotation, which can be better seen from the attached video clip in the SI 2. Clockwise and anticlockwise rolling rotation (about the X-axis) was obtained by interchanging the phase on the electrodes.

The in-plane rotation process was continuous so long as the rotational fields were activated. However, out-of-plane rotation only lasted for one to two minutes. This is because during rolling pitch rotation, the cell was pushed down onto the bottom surface causing it to stop rotation after the stated time period, and the oocyte could only roll a horizontal distance as confined by the chamber dimensions.

In a similar manner to yaw rotation, higher potential amplitude causes faster pitch rotation. The effect of varying buffer medium conductivity was also investigated for rolling pitch rotation rate and the results are shown in Fig. 9. Looking into both Fig. 7 and Fig. 9, we see that the medium conductivity has the same effect on rotation regardless of the rotation axis: higher conductivity increases the rotation rate (owing to the reduced medium viscosity at higher conductivities). The most noticeable difference lies in the frequency range in which the rotation occurs (peaking at around 80 kHz, and dropping to zero at just over 1 MHz). This frequency difference is attributed to the different local electric field magnitude generated by application of the potentials to the two different configurations of electrodes for yaw and rolling pitch rotations, whereby higher electric field magnitude has been shown to reduce the peak rotation frequency (see Fig 6).

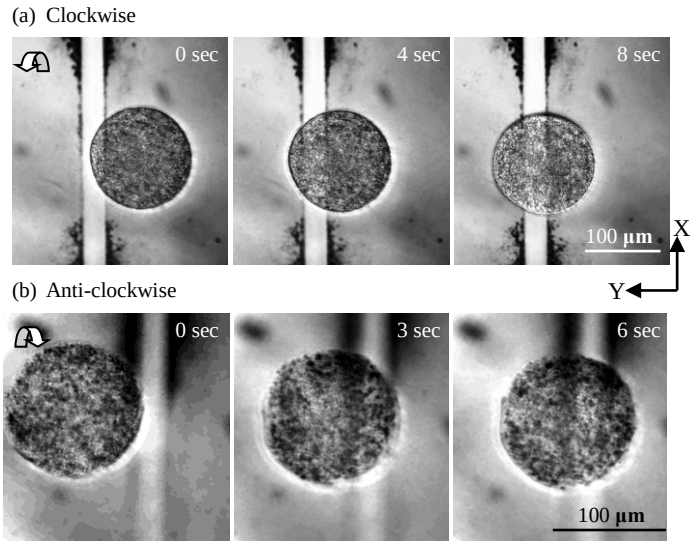

Fig. 8: Snapshot of individual bovine oocyte rolling rotation in experiment. (a) Clockwise rotation. (b). Anti-clockwise rotation with larger view of the oocyte (note: lysed oocyte). Settings are 10 V, 40 kHz and 50 °phase shift between the two bottom electrodes.

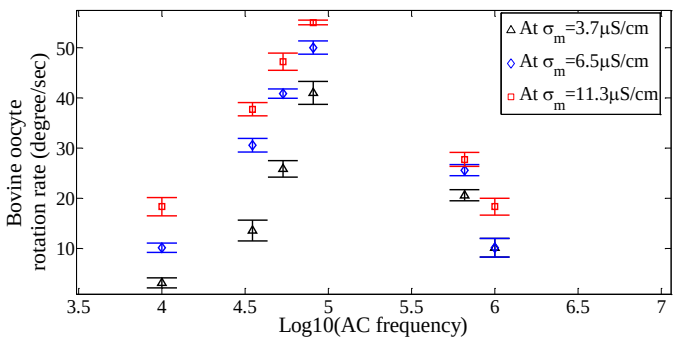

Fig. 9: ZP-free bovine oocyte rolling rotation rate in relation to the conductivity of buffer medium and the applied frequency in experiment. Here the ac potential amplitude is fixed at 10 V. Based on N=4, n=3.

Effect of zona pellucida (ZP)

Since our direct motivation is to remove DNA from bovine oocytes, depending on the method employed, oocytes with either an intact or removed ZP may need to be manipulated. Therefore, we compared the rotation rate for ZP-intact and ZP-free oocytes. Considering the rotations about both axes have no essential difference, oocyte rotation data were collected for in-plane rotation only and the results shown in Fig. 10. Though ZP-intact oocytes had slightly slower rotation rates compared to ZP-free oocytes, the difference is negligible. Removal of the ZP does not substantially reduce the size and weight of the oocyte; from Eqn. (1) we can deduce the rotation torque remains almost the same. Therefore, the dielectric property of the ZP-free oocyte is nearly equivalent to the ZP-intact oocyte, indicating a possible electrical equivalency between the cytoplasm/cell membrane structure and its surrounding ZP. From the data in Fig. 10, under an amplitude of 10 V, for example, a ZP-intact oocyte can have consistent rotation at ~20 ⁹s at 1 MHz. This setting may be used for control of cell rotation in enucleation/injection applications.

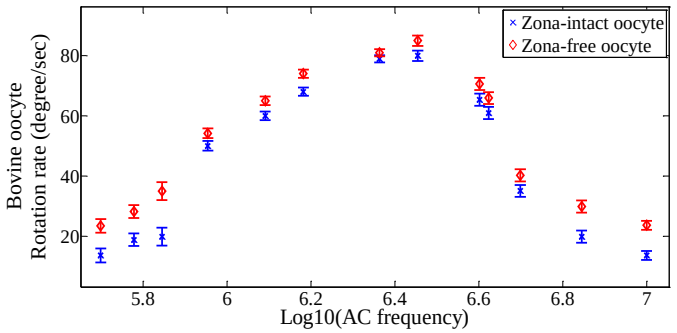

Fig. 10: Comparison of the in-plane rotation rate for ZP-intact and ZP-free bovine oocytes. Here the ac amplitude is fixed at 10 V. Based on N=4, n=3. Medium conductivity used is σ_m=3.9 μS/cm.

From Figs. 6, 7, 9, and 10, the rotation rate spectra about the two orthogonal axes have the same pattern with a single peak Gaussian-like shape. The pattern is expected to be the same as the cell can be considered here as essentially a 3D homogeneous entity. The curves have only one peak with no Maxwell Wagner (MW) relaxation [55, 56], indicating the bovine oocytes can be reasonably approximated by solid sphere model rather than a shell model, and are more polarizable than the medium, as predicted by the established theory [57-59]. Furthermore, this solid sphere model can hold in consideration of the electrical equivalency between the oocyte cytoplasm/membrane structure and its surrounding ZP, which was found earlier (see Fig. 10).

It should be pointed out that although bovine oocytes were used in experiment to demonstrate cell rotation, the biochip platform is readily available for other larger or smaller entities, like nematodes, yeast cells, microbeads, molecules, even DNA and proteins. These entities have different properties including size, structure, dielectric coefficients, and morphologies, than bovine oocytes, thus they may have different rotation rates, which could be predicted by the established theory [60] and validated by experiment using this biochip platform. Note that according to Eq. (1), DEP torque is proportional to R^3 of the cell, which means that for smaller bio-particles (e.g., a blood cell) the DEP torque becomes much smaller. To generate a DEP torque comparable for bigger cells (e.g., bovine oocytes), it is necessary to increase the electric field. However, Eq. (4) indicates that particle size is theoretically not a contributing factor that affects the rotation speed. This means in principle there is no need to scale up the electric field to generate enough DEP torque for rotating smaller cells. A valuable feature of this biochip lies in its open top, which allows additional function modules to interface with the chamber and rotating entities. For example, cell sorting microfluidic channels can be added on top of the biochip with orifices overlapping the chamber to facilitate the loading/unloading of individual cells.

Cell lysis is nontrivial in practice. Three possible reasons can contribute to this happening. One is the electric field magnitude. We conducted simulations in COMSOL and found that the peak magnitude (data not shown here) occurs in the center region of the biochip chamber for in-plane rotation, and in the region above the bottom electrodes' gap for rolling pitch rotation, with a value

of 3×10^4 V/m and 1.6×10^4 V/m respectively for an applied potential amplitude of 10 V. Previously reported work of DEP-facilitated cell fusion [52, 61] and electroporation [34, 62] offers clues that this continuously-applied field is strong enough to induce high and potentially damaging cell membrane permeability. The second possible reason is related to the physical property of the cytoplasm under high frequency excitation. In a recent tutorial paper [63], it was mentioned that a rotating cell sample lysed in ultrasonic standing-wave fields. Likewise, under a high frequency electric field, it may be possible for oocytes to have undergone a similar process of breaking up into fragments as observed in these experiments; especially as our cells are simultaneously subjected to the electric field-induced rotation which is an additional physical factor that may contribute to lysis. To minimize cell lysis in practice, a proper combination of applied potential amplitude and frequency is required. For example, two combinations (10 V and 500 kHz during in-plane rotation, and 10 V and 40 kHz during out-of-plane rotation) could be recommended for rotating bovine oocytes based on the experimental results. Therefore, the data in this paper could also be a good reference point to determine proper parameters for other types of cells or particles.

The third possible reason for cell lysis is related to Joule heating. DEP is known to generate a various amount of heating, such as Joule heating, depending on application-specific physical parameter values [64]. Excessive heating is a factor that can affect cell viability. In experiment, we have not measured the temperature change in the medium since the main purpose was to demonstrate rotation. However, no obvious effects of media heating were observed (such as gassing or media turbulence due to convection), and previous work using similar electric field magnitudes and frequencies with the same buffer media and oocytes did not result in any observed heating effects or reduction in cell viability [52]. Even so, we plan to measure temperature variation in future experimental work.

In experiment, we had some noteworthy observations. At low ac frequencies (less than 10 kHz), the electrodes started to corrode and the electrochemical reactions generated bubbles, which should be avoided. Another general observation was that during rolling pitch rotation oocytes tended to simultaneously sink to the bottom electrodes, while this did not happen for in-plane rotation. Through FEA simulations in COMSOL, it was found that there is a DEP drag force pulling the oocyte to the bottom of the chamber for rolling pitch rotation, but not for in-plane rotation. To counter the resulting drag force, extra care should be taken to optimize the geometry design of the bottom electrodes (also an aim of our future work).

Currently, we manually control the external ac potentials for control of the rotating electric field and thus cell rotation. This includes start-stop, direction, and rate of the rotation. Though it is not a problem for demonstration purpose in this paper, manual operation has been one of the most important barriers that hamper us from controlling the rotation continuously and in a closed loop for future cell injection/enucleation. To address this problem, we intend to leverage advances in micro-electronics to make a PC-controllable miniature circuit board that can replace the functions of the currently adopted function generator.

Furthermore, we currently measure the rotation rate or orientation angle offline, which could be improved upon in future as well. To make the control closed-loop, it is necessary to obtain the instantaneous orientation angle as feedback information and thus requires an online method of constantly tracking the cell rotation. This could be accomplished in a manner somewhat similar to what has been done in our labs before [65], using a similar microscopy imaging system but developing a real-time image-based algorithm to measure the cell orientation. Once we are able to control the rotation by computer and in a closed loop, in combination with the standard existing Cartesian microscope stage, the 3D cell rotation biochip platform could be an enabling manipulation tool for many interesting biological studies.

Conclusions

An ac electric field-based biochip platform is constructed by a mixture of fabrication methods via standard lift-off process and micro-milling. Within the sub-mm square chamber of the biochip, bovine cells are demonstrated to be controlled to achieve rotation about two orthogonal axes respectively. The rotation direction and rate are controlled via varying a set of parameter options; namely by changing the ac potentials amplitude, frequency, and phase shift, and cell medium conductivity. Based on experimental observations, we recommend two combinations (10 V and 500 kHz during in-plane rotation, and 10 V and 40 kHz during out-of-plane rotation) for consistent and stable rotation of bovine oocytes with a rotation rate up to 40 °/s. Using a 30 Hz video sampling frequency, the measurable angle change between two successive frames can be as small as 0.57 °. Through the obtained rotation rate spectra, it was found that bovine oocytes could be treated as a solid sphere model and there seems to be no practical difference for ZP-intact and ZP-free oocyte rotational spectra, demonstrating the capability of using this biochip platform to characterize cell dielectric properties. Once closed-loop control by a computer is achieved, the biochip platform can be made more powerful in conjunction with extra function modules, which are facilitated by the simple, transparent, and open-top structure of the chip. In summary, this 3D cell rotation platform offers many opportunities in manipulating and studying single cells or cell populations, other organisms, and particles in 3D space.

Acknowledgements

The authors would like to thank Gary Turner, Helen Devereux and Julian Murphy for technical assistance, as well as Alice Chibnall and Zach McLean for supplying oocytes. Financial support for P. Benhal was provided by the Dept of Mechanical Engineering, University of Canterbury. W. Wang is supported by NSFC (No. 61376120), One-Thousand Young Talent Program of China, and National Key Scientific Instrument and Equipment Development Project (No. 2013YQ19046701).

Notes and references

[a]*Department of Mechanical Engineering, University of Canterbury, Christchurch, New Zealand*
[b]*Department of Electrical and Computer Engineering, University of Canterbury, Christchurch, New Zealand*
[c]*AgResearch Ruakura Research Centre, Hamilton 3240, New Zealand*
[d]*Department of Precision Instruments, Tsinghua University, Beijing, China 100084*

Supplementary information:

1. Methods. PDF file provides supporting information for image processing methods to track cell rotation.

2. Video. The video file provides edited clips of 3D rotation of bovine oocytes.

1. N. Aubry and P. Singh, *Influence of particle-particle interactions and particles rotational motion in traveling wave dielectrophoresis.* Electrophoresis, 2006. **27**(3): p. 703-15.
2. S. I. Han, Y. D. Joo, and K. H. Han, *An electrorotation technique for measuring the dielectric properties of cells with simultaneous use of negative quadrupolar dielectrophoresis and electrorotation.* Analyst, 2013. **138**(5): p. 1529-37.
3. Y. L. Liang, et al., *Cell rotation using optoelectronic tweezers.* Biomicrofluidics, 2010. **4**(4): p. 43003.
4. C.-H. Chiou and G.-B. Lee, *A micromachined DNA manipulation platform for the stretching and rotation of a single DNA molecule.* Journal of Micromechanics and Microengineering, 2005. **15**(1): p. 109.
5. B. Gutierrez-Medina, et al., *An optical apparatus for rotation and trapping.* Methods Enzymol, 2010. **475**: p. 377-404.
6. A. La Porta and M. D. Wang, *Optical torque wrench: angular trapping, rotation, and torque detection of quartz microparticles.* Physical Review Letters, 2004. **92**(19): p. 190801.
7. C. Gosse and V. Croquette, *Magnetic tweezers: micromanipulation and force measurement at the molecular level.* Biophysical Journal, 2002. **82**(6): p. 3314-3329.
8. R. Elbez, et al., *Nanoparticle induced cell magneto-rotation: monitoring morphology, stress and drug sensitivity of a suspended single cancer cell.* PLoS One, 2011. **6**(12): p. e28475.
9. C. Leung, et al., *Three-dimensional rotation of mouse embryos.* IEEE Trans Biomed Eng, 2012. **59**(4): p. 1049-56.
10. M. X. Jiang, et al., *The effects of chemical enucleation combined with whole cell intracytoplasmic injection on panda-rabbit interspecies nuclear transfer.* Zygote, 2004. **12**(4): p. 315-20.
11. U. Zimmermann, et al., *Electromanipulation of mammalian cells: fundamentals and application.* IEEE Transactions on Plasma Science, 2000. **28**(1): p. 72-82.
12. B. Oback and D. N. Wells, *Cloning cattle: the methods in the madness.* Adv Exp Med Biol, 2007. **591**: p. 30-57.
13. B. Oback and D. N. Wells, *Cloning cattle.* Cloning stem cells, 2003. **5**(4): p. 243-56.
14. A. Schurmann, D. N. Wells, and B. Oback, *Early zygotes are suitable recipients for bovine somatic nuclear transfer and result in cloned offspring.* Reproduction, 2006. **132**(6): p. 839-48.
15. P. J. Booth, et al., *Simplification of bovine somatic cell nuclear transfer by application of a zona-free manipulation technique.* Cloning stem cells, 2001. **3**(3): p. 139-50.
16. M. P. Bayona-Bafaluy, G. Manfredi, and C. T. Moraes, *A chemical enucleation method for the transfer of mitochondrial DNA to rho(o) cells.* Nucleic Acids Res, 2003. **31**(16): p. e98.
17. S. L. McElroy and R. A. Reijo Pera, *Noninvasive human nuclear transfer with embryonic stem cells.* CSH Protoc, 2008. **2008**(9): p. pdb prot5040.
18. R. S. Prather, M. M. Sims, and N. L. First, *Nuclear transplantation in early pig embryos.* Biol Reprod, 1989. **41**(3): p. 414-8.
19. P. J. Ross and J. B. Cibelli, *Bovine somatic cell nuclear transfer.* Methods Mol Biol, 2010. **636**: p. 155-77.
20. S. M. Hosseini, et al., *Cloned sheep blastocysts derived from oocytes enucleated manually using a pulled pasteur pipette.* Cell Reprogram, 2013. **15**(1): p. 15-23.
21. L. H. Chau, et al., *Self-rotation of cells in an irrotational AC E-field in an opto-electrokinetics chip.* PLoS ONE, 2013. **8**(1): p. e51577.
22. M. P. Hughes, *AC electrokinetics: applications for nanotechnology.* Nanotechnology, 2000. **11**(2): p. 124.
23. G. Carmon and M. Feingold, *Rotation of single bacterial cells relative to the optical axis using optical tweezers.* Opt Lett, 2011. **36**(1): p. 40-2.
24. T. Arakawa, et al., *High-throughput single-cell manipulation system for a large number of target cells.* Biomicrofluidics, 2011. **5**(1): p. 14114.
25. P. W. Cooley, D. B. Wallace, and B. V. Antohe. *Applications of ink-jet printing technology to BioMEMS and microfluidic systems*. Microfluidics and BioMEMS, 2001. **4560**: p. 177-188.
26. H. Lee, et al., *Integrated cell manipulation system-CMOS/microfluidic hybrid.* Lab Chip, 2007. **7**(3): p. 331-337.
27. F. Arai, T. Kasugai, and T. Fukuda. *3D position and orientation control method of micro object by dielectrophoresis*. Proceedings of the International Symposium on Micromechatronics and Human Science, 1998. p. 149-154.
28. D. J. Bakewell, Morgan, H., *Dielectrophoresis of DNA: time- and frequency-dependent collections on microelectrodes.* IEEE Transactions on Nanobioscience, 2006. **5**(2): p. 139.
29. A. Castellanos, et al., *Electrohydrodynamics and dielectrophoresis in microsystems: scaling laws.* Journal of Physics D: Applied Physics, 2003. **36**(20): p. 2584.
30. M. Zrinyi, M. Nakano, and T. Tsujita, *Electrorotation of novel electroactive polymer composites in uniform DC and AC electric fields.* Smart Materials and Structures, 2012. **21**(6): p. 065022.
31. Y. Huang, et al., *Electrorotational studies of the cytoplasmic dielectric properties of friend murine erythroleukaemia cells.* Physics in Medicine and Biology, 1995. **40**(11): p. 1789.
32. Y. H. Lin, et al., *The application of an optically switched dielectrophoretic (ODEP) force for the manipulation and assembly of cell-encapsulating alginate microbeads in a microfluidic perfusion cell culture system for bottom-up tissue engineering.* Lab Chip, 2012. **12**(6): p. 1164-73.
33. J. Cheng, et al., *Preparation and hybridization analysis of DNA/RNA from E. coli on microfabricated bioelectronic chips.* Nat Biotech, 1998. **16**(6): p. 541-546.
34. J. Cemazar and T. Kotnik, *Dielectrophoretic field-flow fractionation of electroporated cells*. Electrophoresis, 2012. **33**(18): p. 2867-74.
35. T. Heida, W. L. C. Rutten, and E. Marani, *Understanding dielectrophoretic trapping of neuronal cells: modelling electric field, electrode-liquid interface and fluid flow.* Journal of Physics D: Applied Physics, 2002. **35**(13): p. 1592.
36. M. P. Hughes, R. Pethig, and X. B. Wang, *Dielectrophoretic forces on particles in travelling electric fields.* Journal of Physics D: Applied Physics, 1996. **29**(2): p. 474.
37. T. P. Hunt and R. M. Westervelt, *Dielectrophoresis tweezers for single cell manipulation.* Biomed Microdevices, 2006. **8**(3): p. 227-30.
38. R. Pethig, *Dielectrophoresis: using inhomogeneous AC electrical fields to separate and manipulate cells.* Critical Reviews in Biotechnology, 1996. **16**(4): p. 331.
39. R. Pethig, et al., *Dielectrophoretic studies of the activation of human T lymphocytes using a newly developed cell profiling system.* Electrophoresis, 2002. **23**(13): p. 2057-63.
40. R. Pethig, et al., *Electrokinetic measurements of membrane capacitance and conductance for pancreatic beta-cells.* IEE proceedings. Nanobiotechnology, 2005. **152**(6): p. 189-193.
41. M. Sancho, et al., *Interaction between cells in dielectrophoresis and electrorotation experiments.* Biomicrofluidics, 2010. **4**(2): p. 022802.
42. M. S. Talary, et al., *Electromanipulation and separation of cells using travelling electric fields.* Journal of Physics D: Applied Physics, 1996. **29**(8): p. 2198.
43. M. K. Kreysing, et al., *The optical cell rotator*. Opt Express, 2008. **16**(21): p. 16984-92.
44. M. B. Rasmussen, L. B. Oddershede, and H. Siegumfeldt, *Optical tweezers cause physiological damage to escherichia coli and Listeria bacteria.* Appl Environ Microbiol, 2008. **74**(8): p. 2441-6.

45. V. N. Binhi, Y. D. Alipov, and I. Y. Belyaev, *Effect of static magnetic field on E. coli cells and individual rotations of ion-protein complexes.* Bioelectromagnetics, 2001. **22**(2): p. 79-86.
46. J. Zlatanova and S. H. Leuba, *Magnetic tweezers: a sensitive tool to study DNA and chromatin at the single-molecule level.* Biochem Cell Biol, 2003. **81**(3): p. 151-159.
47. H. Yun, K. Kim, and W. G. Lee, *Cell manipulation in microfluidics.* Biofabrication, 2013. **5**(2): p. 022001.
48. P. Benhal. P. Gaynor, J. G. Chase, B. Oback, W. H. Wang, *Dielectrophoresis-based 3D cell rotation through integration of bottom and vertical electrodes.* Proceedings of MicroTAS-2013 conference, 2013: p. 970-972.
49. T. B. Jones, *Basic theory of dielectrophoresis and electrorotation.* IEEE Eng Med Biol Mag, 2003. **22**(6): p. 33-42.
50. X. Wang, R. Pethig, and T. B. Jones, *Relationship of dielectrophoretic and electrorotational behaviour exhibited by polarized particles.* Journal of Physics D: Applied Physics, 1992. **25**(6): p. 905.
51. A. Mao, C. D. Schaper, and R. F. K. Jr, *Nanopatterning using a simple bi-layer lift-off process for the fabrication of a photonic crystal nanostructure.* Nanotechnology, 2013. **24**(8): p. 085302.
52. P. Gaynor, D. N. Wells, and B. Oback, *Couplet alignment and improved electrofusion by dielectrophoresis for a zona-free high-throughput cloned embryo production system.* Med Biol Eng Comput, 2005. **43**(1): p. 150-154.
53. U. Lei, P. H. Sun, and R. Pethig, *Refinement of the theory for extracting cell dielectric properties from dielectrophoresis and electrorotation experiments.* Biomicrofluidics, 2011. **5**(4): p. 44109-4410916.
54. S. Park, et al., *Continuous dielectrophoretic bacterial separation and concentration from physiological media of high conductivity.* Lab Chip, 2011. **11**(17): p. 2893-900.
55. A. Al-Jarro, et al., *Direct calculation of Maxwell stress tensor for accurate trajectory prediction during DEP for 2D and 3D structures.* Journal of Physics D: Applied Physics, 2007. **40**(1): p. 71.
56. X. B. Wang, et al., *Theoretical and experimental investigations of the interdependence of the dielectric, dielectrophoretic and electrorotational behaviour of colloidal particles.* Journal of Physics D: Applied Physics, 1993. **26**(2): p. 312.
57. J. Gimsa, *A comprehensive approach to electro-orientation, electrodeformation, dielectrophoresis, and electrorotation of ellipsoidal particles and biological cells.* Bioelectrochemistry, 2001. **54**(1): p. 23-31.
58. J. Gimsa and D. Wachner, *A polarization model overcoming the geometric restrictions of the laplace solution for spheroidal cells: obtaining new equations for field-induced forces and transmembrane potential.* Biophys J, 1999. **77**(3): p. 1316-26.
59. I. Turcu and C. M. Lucaciu, *Electrorotation: a spherical shell model.* Journal of Physics A: Mathematical and General, 1989. **22**(8): p. 995.
60. H. S. Chuang, et al., *Dielectrophoresis of Caenorhabditis elegans.* Lab Chip, 2011. **11**(4): p. 599-604.
61. U. Zimmermann and P. Scheurich, *High frequency fusion of plant protoplasts by electric fields.* Planta, 1981. **151**(1): p. 26-32.
62. T. Y. Tsong, *Electroporation of cell membranes.* Biophys J, 1991. **60**(2): p. 297-306.
63. M. Wiklund, *Acoustofluidics 12: Biocompatibility and cell viability in microfluidic acoustic resonators.* Lab Chip, 2012. **12**(11): p. 2018-2028.
64. S. Sridharan, et al., *Joule heating effects on electroosmotic flow in insulator-based dielectrophoresis.* Electrophoresis, 2011. **32**(17): p. 2274-2281.
65. S. Johari, et al., *On-chip analysis of C. elegans muscular forces and locomotion patterns in microstructured environments.* Lab Chip, 2013. **13**(9): p. 1699-1707.